The EMBO Journal vol.11 no.3 pp.1155-1164, 1992

Symmetry, flexibility and permeability in the structure of yeast retrotransposon virus-like particles

Nigel R.Burns[1], Helen R.Saibil[2], Nicholas S.White[3], John F.Pardon[1], Peter A.Timmins[4], S.Mark H.Richardson[1], Brian M.Richards[1], Sally E.Adams[1], Susan M.Kingsman[5] and Alan J.Kingsman[1,5]

[1]British Bio-technology Limited, Watlington Road, Oxford OX4 5LY, [2]Department of Crystallography, Birkbeck College, Malet Street, London WC1E 7HX, [3]Department of Zoology, Oxford University, South Parks Road, Oxford OX1 3PS, UK [4]Institut Laue-Langevin, 156X, 38042 Grenoble Cedex, France, and [5]Virus Molecular Biology Group, Department of Biochemistry, Oxford University, South Parks Road, Oxford OX1 3QU, UK

Communicated by T.Blundell

The virus-like particles (VLPs) of the yeast retrotransposon Ty are genetically, structurally and functionally analogous to retroviral nucleocapsids or cores. Like retroviral cores Ty-VLPs package and possibly promote the enzyme activities for reverse transcription and integration, as well as encapsulating the RNA that is the intermediate in retrotransposition. Here we show that Ty-VLPs assemble into symmetrical structures across a broad distribution of particle sizes. This spread of sizes violates the principle of quasi-equivalent packing. In addition, RNase accessibility experiments suggest that these particles form an open structure that does not protect the encapsulated RNA. These features distinguish Ty-VLPs from typical spherical viral capsids in both structure and function.
Key words: retrovirus/transposon/virus structure

Introduction

Both retroviruses and retrotransposons, such as the yeast Ty1 element, replicate via a reverse transcriptase (RT) step followed by an integration reaction that inserts the product of reverse transcription into the host genome (for a recent review see Kingsman and Kingsman, 1988). The RT, integrase (IN) and RNA template are packaged, in both types of element, into a nucleocapsid or core. In the case of retroviruses these nucleocapsids bud from the host cell and in so doing become enveloped in host cell membrane. Within that membrane are the viral *env* glycoproteins which target newly formed virus to another susceptible host cell. In contrast the nucleocapsid of the yeast Ty1 retrotransposon does not bud from the yeast cell, nor does the element encode any membrane glycoproteins. The Ty nucleocapsids are therefore not infectious.

In the case of Ty1, isolated nucleocapsids, called Ty-virus-like particles (Ty-VLPs) have been shown to carry out transposition reactions *in vitro* (Eichinger and Boeke, 1988). These reactions involve both a RT and an IN step. Significantly, mutations that do not affect the integrity of the enzymes but which alter the major nucleocapsid structural protein prevent the *in vitro* reaction suggesting that the structure of the particle is important for the reaction (Eichinger and Boeke, 1988). Similarly, retroviral nucleocapsids also mediate integration *in vitro*. It has been shown that the preintegration complex *in vivo* is a high molecular weight structure including capsid proteins (Bowerman *et al.*, 1989; Roberts and Oroszolan, 1989). Taken together these results suggest that the nucleocapsid may participate in both the RT and IN reactions. Against this notion is the fact that purified retroviral RT and IN proteins are functional *in vitro*, although the efficiency of these systems is difficult to assess (Craigie *et al.*, 1990; Bushman *et al.*, 1990; Katz *et al.*, 1990).

Given that retro-element nucleocapsids are central to the assembly of the components of reverse transcription and integration, and may play a role in the reactions of these components, it is surprising that relatively little is known about their molecular architecture. This paucity of data is due to both the pleomorphic nature of many retro-nucleocapsids and the difficulty in purifying these structures in quantities sufficient for biochemical and physical analyses. We have shown previously that by overexpression of the Ty1 transcription unit we can produce large quantities of Ty nucleocapsids (Ty-VLPs) (Mellor *et al.*, 1985a). This makes Ty1 an attractive model for the study of these structures.

The Ty1 element is ~5.9 kb in length with Long Terminal Repeats (LTRs) of ~340 nucleotides. The major transcript is the full-length 5.7 kb RNA that is both message and intermediate in transposition (Boeke *et al.*, 1985). This transcription unit is divided into two genes. The first, *TYA*, encodes a 50 kDa protein, p1, which is capable of assembly into VLPs (Adams *et al.*, 1987a). Protein p1 is processed by cleavage to the smaller, 46 kDa protein, p2. The cleavage occurs within an immature particle to produce the mature particle of which the major component is p2. The second gene, *TYB*, encodes the enzyme activities: a protease that mediates the p1 to p2 cleavage, IN and RT. *TYB* is expressed via a ribosomal frameshift event that fuses the coding sequences of *TYA* and *TYB* to produce a 190 kDa fusion protein known as p3 (Mellor *et al.*, 1985a). The ratio of p1 to p3 is ~20:1. Presumably, the enzyme activities encoded by *TYB* are incorporated into Ty-VLPs via interactions between the self-assembling p1 protein and the p1 component of p3. Clearly, the *TYA* gene is an analogue of retroviral *gag* genes which encode the structural proteins of retroviral nucleocapsids and the *TYB* gene is an analogue of the retroviral *pol* genes that encode the enzyme activities.

With a view to understanding more of the structure of Ty1 nucleocapsids and their possible role in reverse transcription and integration we have started to analyse the structure of these particles. Using image analysis of electron micrographs, hydrodynamic analysis, neutron scattering and RNA digestions, we show that Ty-VLPs are symmetrical struc-

tures, they show a pronounced variation in size and they are permeable to RNases. These observations suggest that Ty-VLPs perform functions, and assemble via processes, different from those of typical spherical virus capsids.

Results

Ty-VLPs are polydisperse

In initial experiments wild-type Ty-VLPs were expressed at high levels from plasmid pMA91-10 (Figure 1a) and

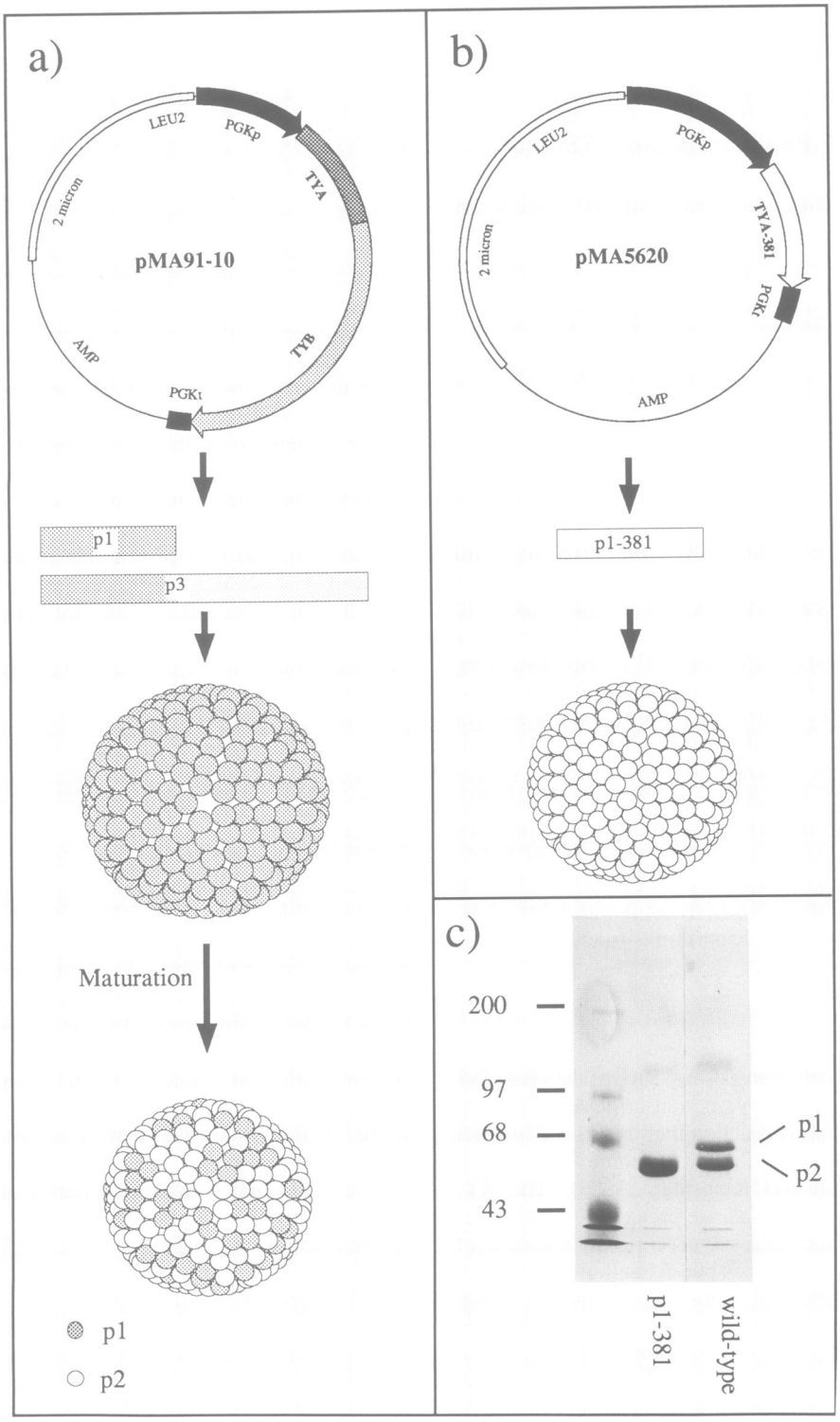

Fig. 1. Schematic diagram of formation of Ty-VLPs. (**a**) Wild-type VLPs were expressed from transcripts of *TYA* and *TYB* from plasmid pMA91-10. This plasmid therefore encodes proteins p1 (from *TYA* transcript) and p3 (from *TYA:TYB* transcript) Particle formation occurs from the assembly of p1. A subsequent maturation step results in the proteolytic cleavage of p1 such that the protein shell of wild-type VLPs is comprised of p1 and its product, p2, in approximately equimolar amounts. (**b**) p1−381 VLPs are expressed from plasmid pMA5620 encoding the first 381 amino acids of p1. This protein forms particles in the absence of *TYB* products. (**c**) SDS−polyacrylamide gel of wild-type Ty1 and p1−381 VLPs purified as described in the text. The minor bands seen running above the main Ty bands correspond to dimers (and higher species), which do not dissociate even in the presence of SDS and 2-mercaptoethanol.

purified to near homogeneity (Figure 1c). Electron microscopy of negatively stained preparations of these VLPs showed individual particles as stain-excluding shells of variable diameter (Figure 2a). Five micrographs, of wild-type particles embedded in negative stain over holes in the support film, were digitized and the radii of 109 particles were estimated and plotted as a histogram (Figure 2b). This showed the wild-type particles to be highly polydisperse, ranging in radius from 15 to 39 nm. The largest particles were often malformed or distorted into irregular shapes, and in these cases could not be measured. It was difficult to assess whether the heterogeneity was an intrinsic property of Ty-VLPs, or whether it could be attributed to varying stages of particle maturity. The size variation and deformities precluded further structural analysis. We therefore used a simpler system in which a truncated version of the *TYA* gene was overexpressed. We have shown previously that the expression of a modified Ty transcription unit (*TYA-381*) leads to the formation of VLPs composed of a single protein species p1−381, comprising the first 381 amino acids of p1. Protein p1−381 has a C-terminus close to the C-terminus of p2, the major protein of mature Ty-VLPs (Figure 1c). Such p1−381 VLPs show the same shell-like morphology as the mature wild-type particles and retain the ability to package their cognate RNA (unpublished data). Therefore, p1−381 VLPs retain the essential features of Ty-VLP structure, and yet provide a simpler system for analysis since the entire population is composed only of a single protein subunit.

The size distribution of p1−381 VLPs was measured from electron micrographs of negatively stained particles suspended over holes in the support film. They occupy a smaller size distribution than the wild-type particles, ranging from 11 to 16 nm, which overlaps with the lower end of the wild-type size distribution (15−39 nm) (Figure 2c and d). Large distorted structures were not seen in the p1−381 preparation. Thus, polydispersity is an intrinsic property of Ty-VLPs, even when they are composed of a single

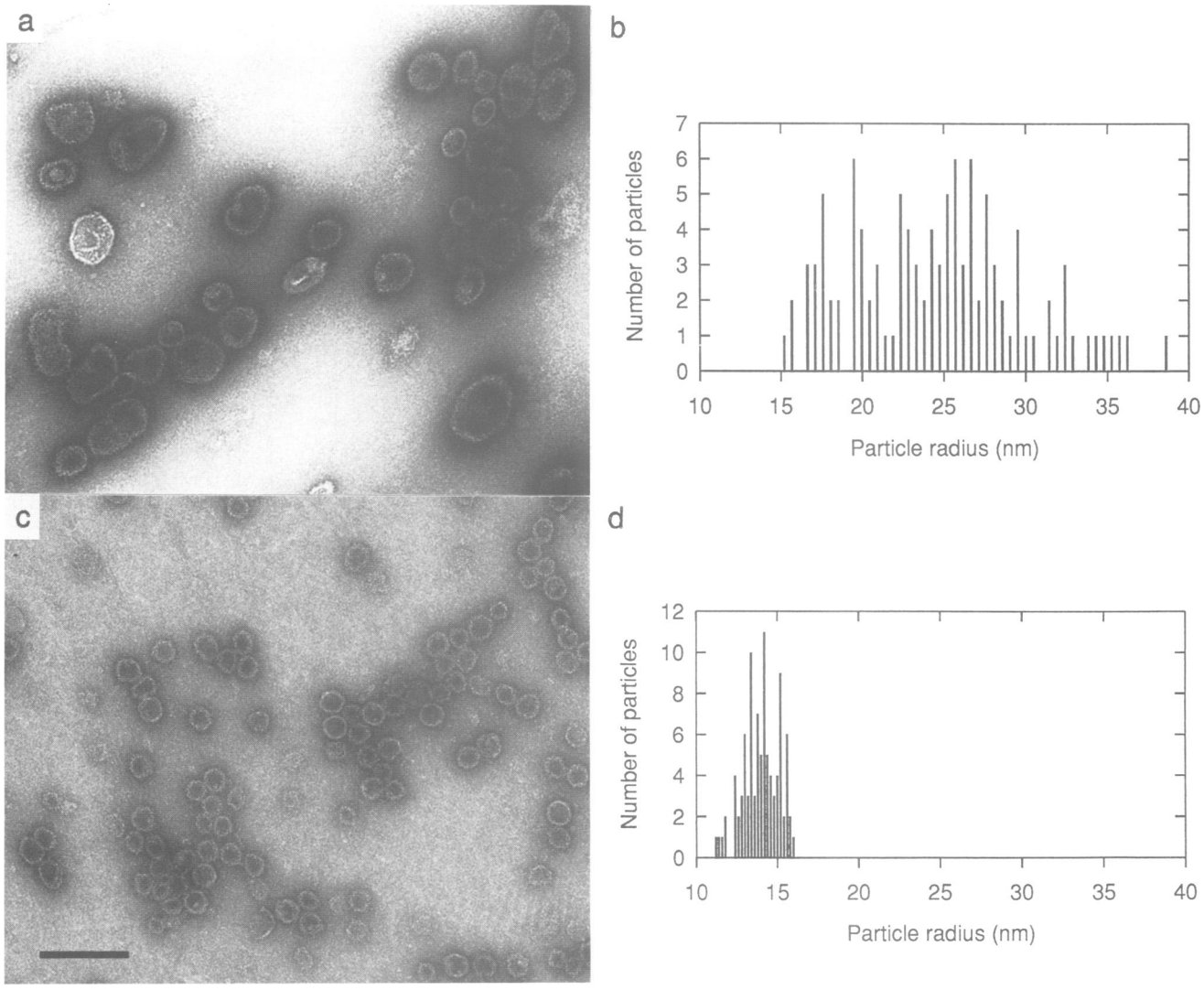

Fig. 2. Electron microscopy of negatively stained Ty-VLPs. (**a**) Negative stain electron microscopy of wild-type Ty1-15 VLPs suspended over a hole in a perforated carbon support. The protein shells appear as light rings embedded in a dark area of stain. Note the extreme variations in size. The larger particles are sometimes malformed as heart shapes. (**b**) Histogram of particle radii in a sample of 109 wild-type VLPs. (**c**) Negative stain electron microscopy of p1−381 VLPs as above. Note the more restricted size range as compared with the wild-type particles. (**d**) Histogram of particle radii in a sample of 95 p1−381 VLPs. Magnification bar, 100 nm.

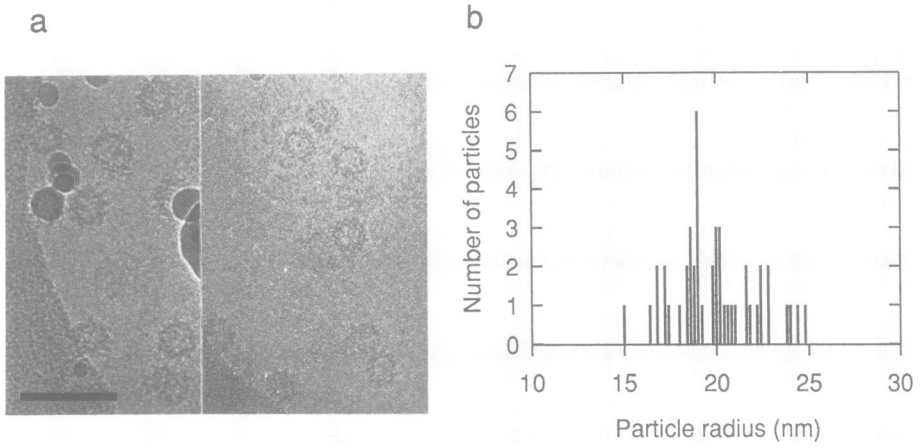

Fig. 3. Cryo-electron microscopy of p1−381 VLPs. (**a**) Frozen-hydrated p1−381 VLPs imaged by low dose cryo-electron microscopy. The unstained protein shells are darker than the surrounding vitreous ice. Note the spiky texture of the particles, which is more clearly imaged than by negative stain of the same sample (Figure 2c). Magnification bar 100 nm. (**b**) Histogram of 46 frozen-hydrated p1−381 VLPs. Comparison with particles negatively stained on holes shows 30% larger radii for the frozen-hydrated particles.

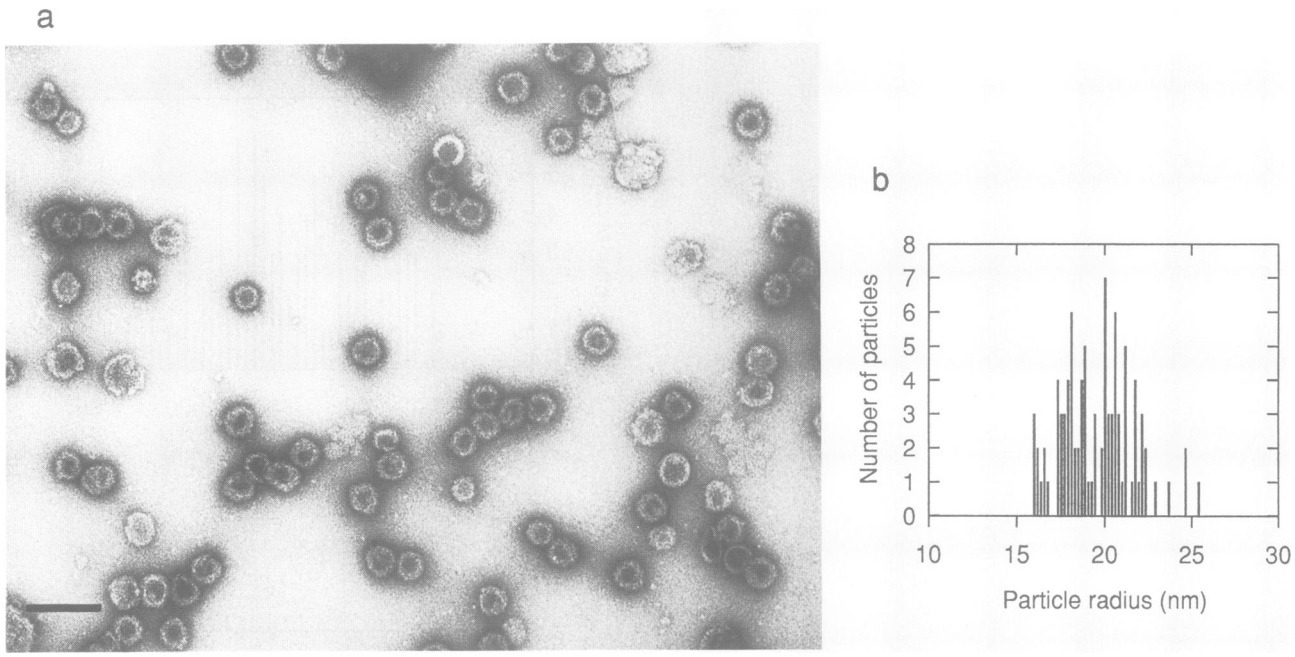

Fig. 4. Electron microscopy of negatively stained p1−381 VLPs. (**a**) Low dose negative stain electron microscopy of p1−381 VLPs imaged on a thin carbon support film. The shell is more clearly visualized than by negative staining on holes, but the particles are not as well preserved as by cryo EM. Magnification bar 100 nm, (**b**) Histogram of the sizes of 93 particles. The distribution matches extremely well with that for cryo EM (Figure 3b).

molecular species. Because the size range of p1−381 is more restricted, and the particles are less prone to deformation, these particles are amenable to structural analysis.

The process of negative staining can introduce distortions into biological structures. The imaging method that gives the best approximation to the native, hydrated protein structure of virus particles is cryo-electron microscopy (cryo EM) of unstained specimens embedded in vitreous ice (Dubochet *et al.*, 1988). Although the contrast between protein and ice is very low, cryo-electron micrographs of p1−381 VLPs show very distinct structural features, notably the presence of spikes projecting from the particles (Figure 3a). Particles with circularly symmetric profiles, suspended in ice and free of contacts with the carbon film or with other particles, were individually digitized for analysis. The size distribution of 46 frozen hydrated particles (Figure 3b) confirmed the polydispersity of p1−381 VLPs but with 30% larger scale, due to shrinkage of particles when negatively stained over holes.

Ty-VLPs form symmetrical structures

The unusual polydispersity of p1−381 VLPs led us to question whether they were comprised of symmetrically arranged subunits or of random, unordered aggregates. We approached this by investigating whether any of the particles showed rotational symmetry. Since the low signal to noise

ratio of the cryo EM images makes their analysis difficult, we obtained low dose negative stain images of p1−381 VLPs on thin carbon films (Figure 4a). This gave good quality particle images with a size distribution matching very well with the cryo EM data (Figure 4b). Although the spikes are less distinct, the higher contrast and signal-to-noise facilitated the symmetry analysis. Particles with circularly symmetric profiles, free of obvious distortion, were selected for image processing. These were assessed for rotational symmetry by computing the rotational auto-correlation of the particle shell in digitized images of 93 particles. Electron micrographs of these particles show their three-dimensional structure projected onto the plane of the film. The particle orientation determines which projection is seen. In ~10% of the particle images, peaks in the auto-correlation function were seen at rotation angles of 36°, 72°, 108°, 144° and 180°, demonstrating 10-fold symmetry about the axis of view (Figure 5). This is consistent with a three-dimensional structure with 5-fold symmetry, projected along a 5-fold axis, resulting in superposition of top and bottom faces to give an apparent 10-fold symmetry in the image. The remaining particles did not show consistent maxima in the rotational auto-correlation, suggesting that none of their symmetry axes were aligned with the direction of view, or that they exhibited no particular symmetry. The widespread presence of rotational symmetry suggests that formation of p1−381 VLPs of all sizes is the result of the symmetrical assembly of subunits. To improve the structural detail, images of two

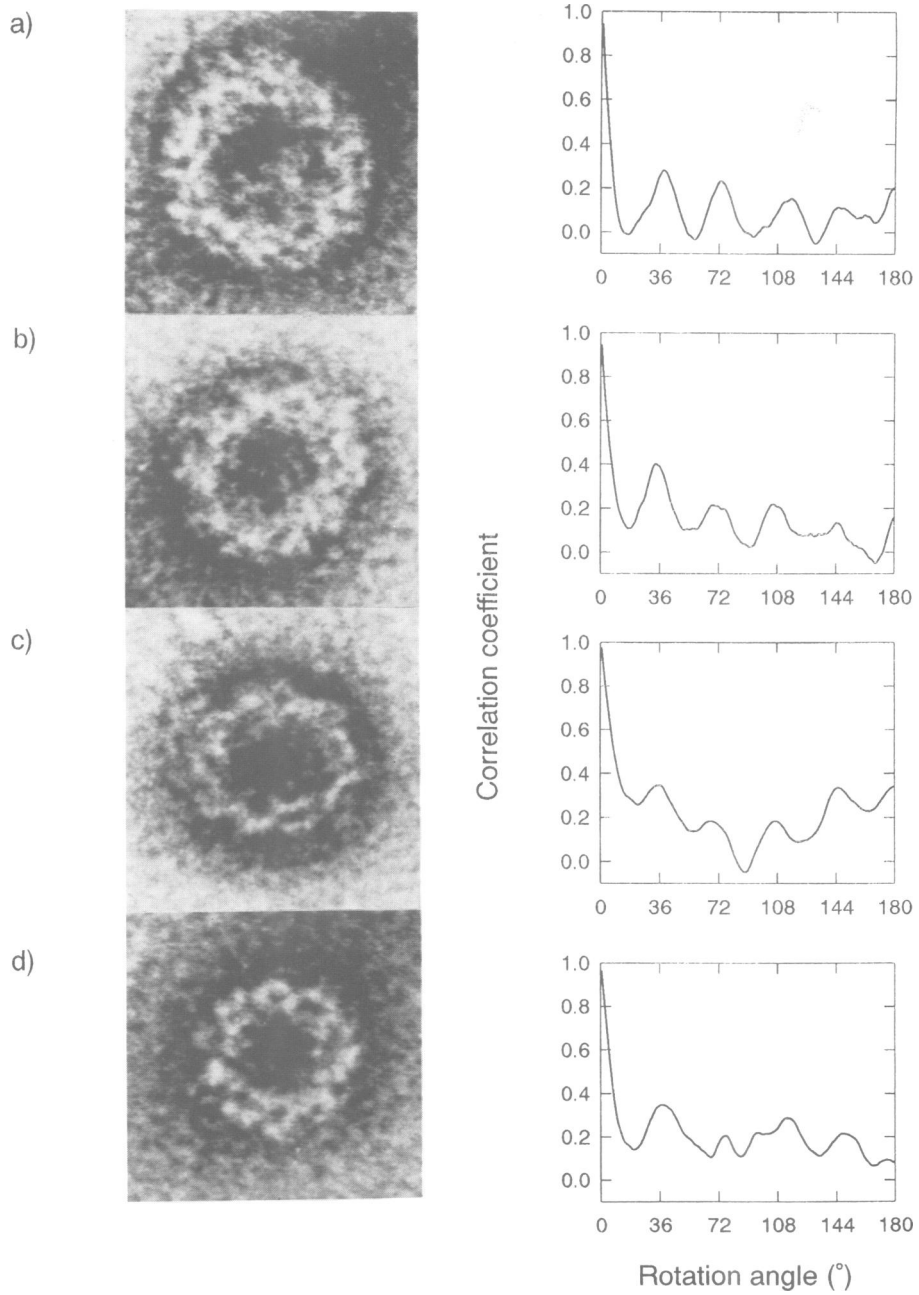

Fig. 5. Image analysis of p1−381 VLPs. Enlarged images and autocorrelations shown in (**a**−**d**) are of particles with outer radii 22.4, 20.3, 17.0 and 17.0 nm respectively. The particle shells appear as light areas surrounded by dark stain. Peaks in their rotational correlations at angles of 36, 72, 108, 144 and 180° indicate the presence of 10-fold symmetry in the images, consistent with 5-fold symmetry in the particles.

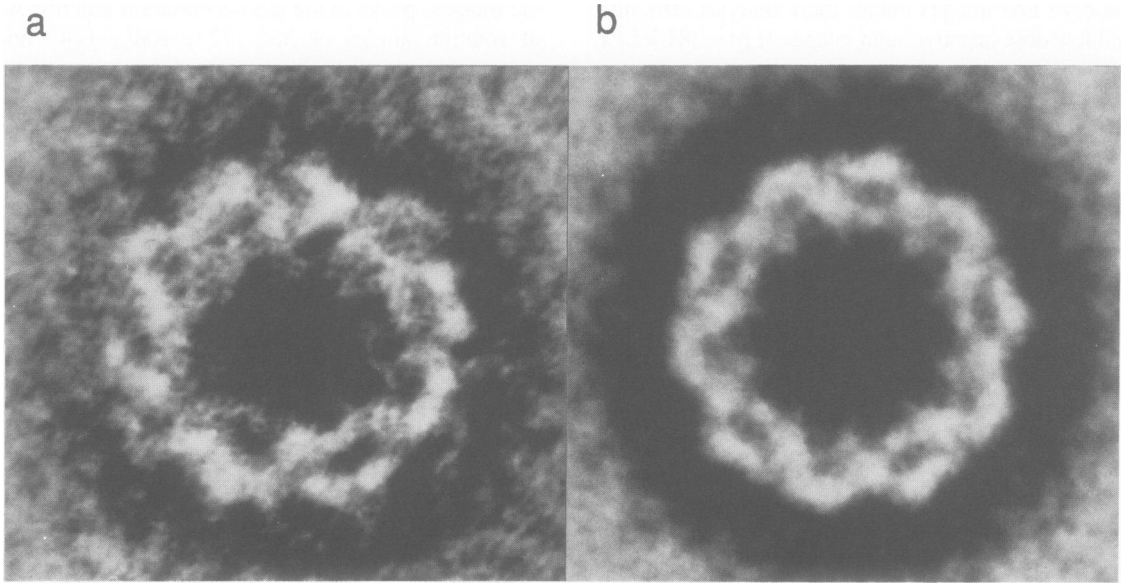

Fig. 6. Image enhancement of p1−381 VLPs. (**a**) The averaged image of two particles of radius 17 nm (Figure 5c and d) after alignment in position and rotational angle. The appearance of 10 loop-like features around the shell is enhanced. (**b**) Five-fold average of (a), further enhancing the loop features of the projected shell structure.

particles of the same diameter were averaged after alignment by rotational cross-correlation. This enhanced the appearance of the projected shell density, making 10 loops of stain excluding structure more distinct (Figure 6a). This averaging was further improved by 5-fold rotational averaging, a procedure justified by the evidence for 5-fold symmetry (Figure 6b). The resulting structure closely resembles some of the cryo EM particle images (Figure 3a).

Solution structure of Ty-VLPs

In order to understand further the structure of Ty-VLPs we sought to establish the average subunit composition of the particles and locate the RNA within the structure. The composition and mass of purified p1−381 VLPs were examined by UV absorbance and analytical centrifugation. From the known amino acid composition and the ratio of absorbances at 260 nm and 280 nm, the RNA content was found to be 15% (w/w) and the partial specific volume to be 0.692 cm^3/g. Consistent with the observed polydispersity, a single, broad peak was readily detectable in the Schlieren pattern on analytical ultracentrifugation of p1−381 VLPs. This yielded a sedimentation coefficient $S_{20,w}$ of 115S (Figure 7). Photon correlation spectroscopy at 90° was used to determine the diffusion coefficient, $D_{20,w}$, as $6.67 cm^2/s \times 10^{-8}$. These parameters were used to calculate the molecular weight of p1−381 VLPs as 14.1 MDa by use of the Svedberg equation (Svedberg and Pederson, 1940). This weight-averaged mass corresponds to a weight-average of 300 protein subunits per particle and 4.5 kb of RNA per particle.

Although there seems to be a general consensus that retroviral RNA is encapsulated within the core particle, this conclusion is not based on any direct biochemical or physical analyses. Since Ty RNA cannot be discriminated easily by electron microscopy, additional methods were required to locate the RNA relative to the VLP protein. Low angle neutron scattering has been successfully employed to determine the spatial relationship between nucleic acid and

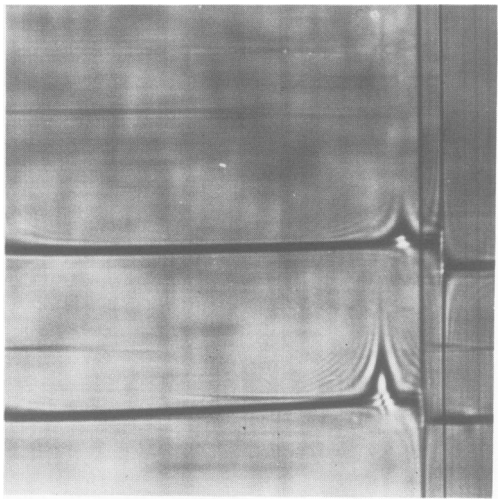

Fig. 7. Analytical ultracentrifugation of p1−381 VLPs. Schlieren pattern of p1−381 VLPs subjected to analytical ultracentrifugation at a concentration of 0.46 mg/ml (top) and 0.94 mg/ml (bottom). The photograph was taken 24 min after reaching a speed of 7928 r.p.m.

protein in a number of systems (for a review see Timmins and Zaccai, 1988). This procedure exploits the differential scattering contrast between these two macromolecules in solutions containing varying H_2O/D_2O mixtures. Moreover, radial density profiles can be obtained from model fitting to neutron scattering curves. We therefore employed low angle neutron scattering to examine the location of the RNA and to derive a radial density profile for p1−381 VLPs in solution. Scattered intensity of p1−381 VLPs in the Guinier region (Guinier and Fournet, 1955) yielded radius of gyration values of 19.2 ± 0.47 nm and 20.5 ± 0.38 nm in 0% and 100% D_2O respectively. The shift in the radius of gyration with scattering contrast indicated that the higher scattering density material (i.e. RNA) was inside the protein shell. The weight-averaged molecular weight derived from the intensity

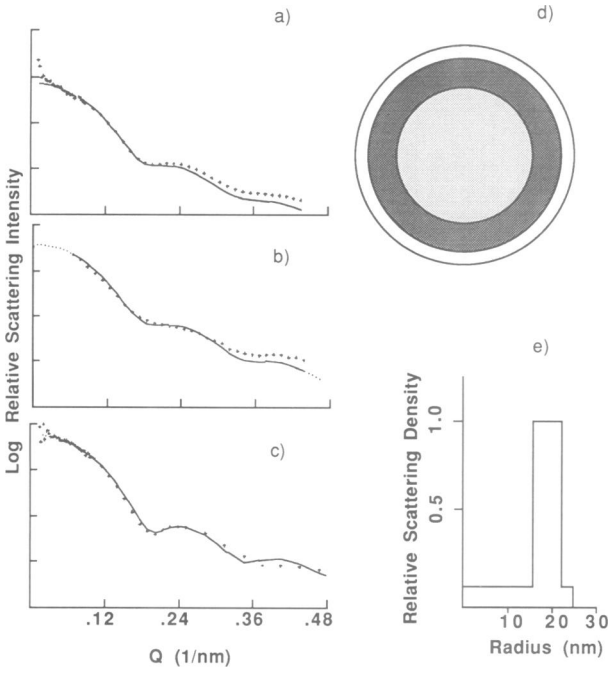

Fig. 8. Analysis of small angle scattering data from solutions of p1−381 VLPs. (**a**−**c**) radially averaged neutron scattering profiles (crosses) from p1−381 VLPs in (a) 0%, (b) 70% and (c) 100% D_2O. The solid line in each panel represents the theoretical scattering profile generated by models consisting of concentric shells of varying scattering densities. The H_2O/D_2O ratio of the solvent determines the relative scattering densities of the protein and RNA moieties, while the shell dimensions remain constant. (**d**) diagrammatic, and (**e**) graphical, representations of the radial distribution of scattering used to compute the fit to the data collected in 100% H_2O. The chemical nature of each shell's contents is indicated by the scattering density as a function of contrast; hence the central cavity (0−15.5 nm) which has zero density at ~70% D_2O corresponds to RNA. The two outer shells (15.5−250 nm) corresponds to protein. The bulk of the protein is modelled as a 6.5 nm shell between the radii 15.5 and 22 nm.

at zero angle (Jacrot and Zaccai, 1981) was 13.9 MDa, in good agreement with the value of 14.1 MDa determined via the Svedberg equation.

The nature of the neutron scattering curves also gives information on size distribution. A monodisperse population of particles with spherical shells would give rise to discrete maxima and minima. Since the electron micrographs show that p1−381 VLPs are circular in projection, the smearing of the neutron scattering curves confirms that they are polydisperse in solution.

Model calculations were used to fit homogeneous, spherical shells of differing scattering density to the low angle scattering curves. Models were constrained by the experimentally determined R_g and an outer radius of 25 nm derived from the distance distribution, which was also calculated from the experimental data (Glatter, 1982). The best results were obtained for the models shown in Figure 8, in which the model corresponded to an RNA-containing central lumen of radius 15.5 nm, surrounded by a protein shell of 6.5 nm in thickness, similar to that seen in the electron micrographs. The 6% of the total protein mass between 22 and 25 nm is presumed to arise from the radial projections seen in the cryo-electron micrographs but not clearly resolved in negative staining.

There is therefore very good agreement between the data obtained from electron microscopy, neutron scattering and hydrodynamic analysis.

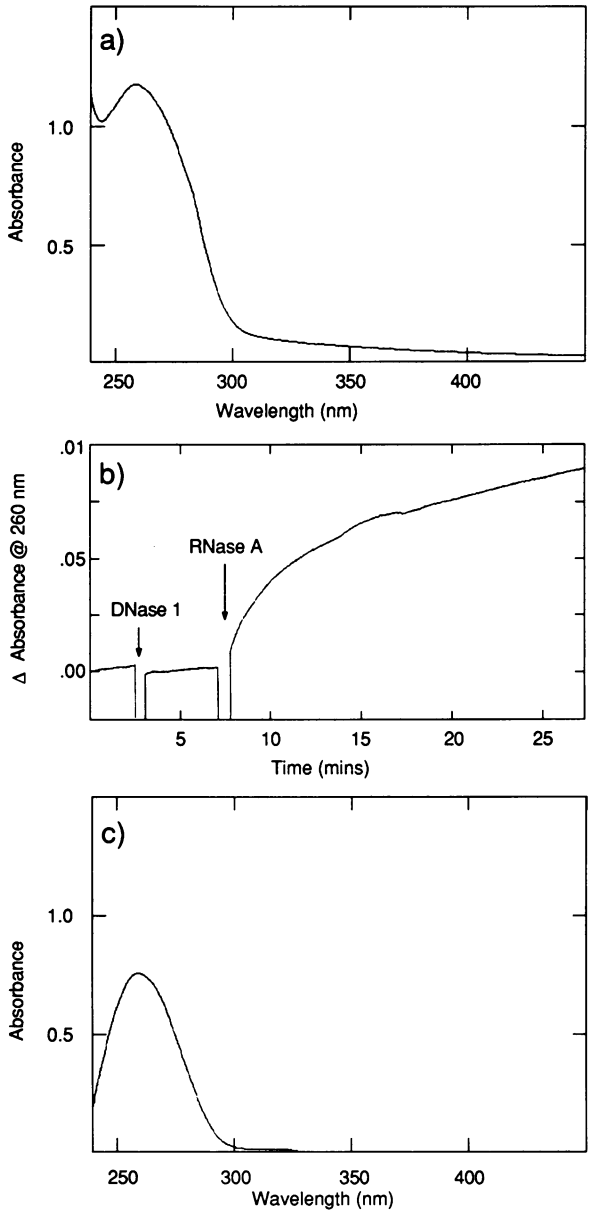

Fig. 9. Susceptibility of Ty RNA to RNase A. (**a**) UV absorbance spectrum of p1−381 VLPs. The spectrum shows features of both protein and nucleic acid absorbtion. (**b**) The effect on the absorbance at 260 nm of p1−381 VLPs was measured following the addition of DNase 1 and RNase A to 1 μg/ml at the times indicated. Note the rapid rise in OD_{260} on the addition of RNase A. (**c**) UV spectrum of the supernatant of p1−381 VLPs treated with RNase A and then subjected to ultracentrifugation. This spectrum is similar to that of protein-free nucleic acid.

Ty RNA is packaged but not protected

One of the major roles of viral capsids is generally believed to be protection of the genome. To examine whether this is a role performed by Ty-VLPs and to confirm the location of the RNA, we examined the susceptibility of VLP-associated RNA to exogenously added nucleases.

We have shown by Northern blotting that p1−381 VLPs package their cognate RNA (unpublished data). A simple means of assessing degradation of this Ty RNA is by measuring the decrease in hypochromicity of the nucleic acid absorption peak at 260 nm. Such an increase in absorbance arises from the loss of base pair stacking. When DNase I is added to p1−381 VLPs no increase in absorbance at

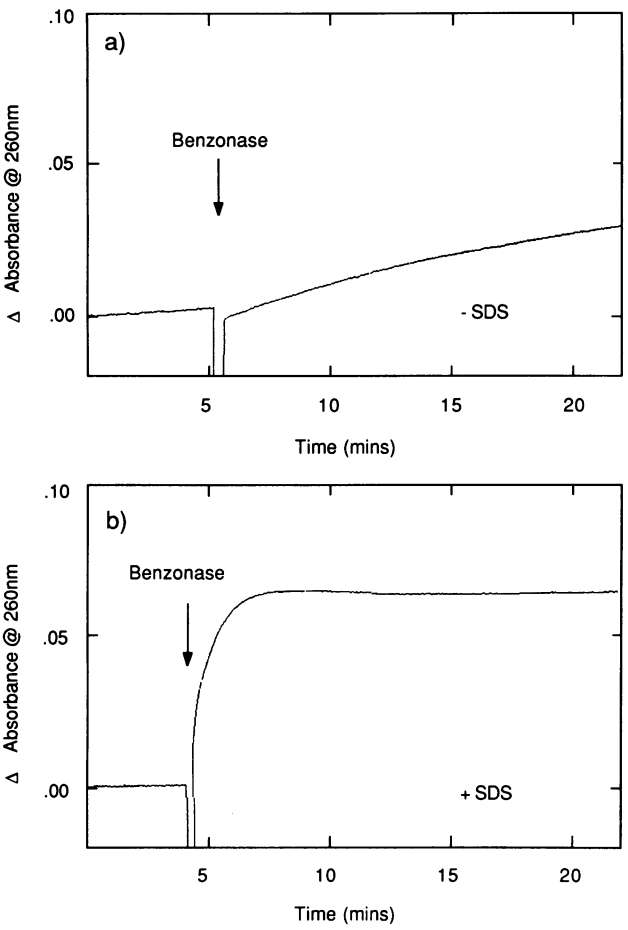

Fig. 10. Susceptibility of Ty RNA to Benzonase. (**a**) Change in OD_{260} of native p1−381 VLPs on the addition of Benzonase (an RNA/DNA nuclease) to native p1−381 VLPs. Note that the addition of the nuclease at the time indicated results in a slow rise in OD_{260}. (**b**) Change in OD_{260} of p1−381 VLPs previously dissociated with 0.075% SDS. Note that by contrast with (a), the addition of Benzonase results in a very rapid increase in OD_{260}.

260 nm is observed (Figure 9b) as expected. In contrast, if pancreatic RNase A is added, a rapid rise in the absorbance at 260 nm occurs, indicating extensive hydrolysis of the Ty-RNA (Figure 9b). If untreated VLPs are sedimented by ultracentrifugation, very little absorbance is seen in the supernatant (not shown). By comparison, if VLPs treated with RNase A are sedimented, the supernatant shows the absorbance profile expected for free nucleotides (Figure 9c). Therefore it appears that the particulate nature of the Ty-VLPs is preserved even though the degraded RNA is not retained within the particle.

Taken together with the data from the neutron scattering, the susceptibility of Ty-VLP RNA to RNase A, a protein of 13.7 kDa with a diameter of 2−2.5 nm, suggests that the protein shell is porous. If these pores are of a defined size then the RNA should be refractile to nucleases whose radius is greater than the pore. Benzonase, a DNA/RNA endonuclease from *Serratia marcescens* has a molecular weight of 30 kDa, which equates to an unhydrated sphere of 4 nm in diameter. Addition of Benzonase to p1−381 VLPs results in a very slow increase in absorbance at 260 nm, even in the presence of sufficient enzyme to degrade rapidly all the RNA (Figure 10a). p1−381 VLPs can be dissociated in 0.075% SDS (unpublished observations) and under these conditions Benzonase retains at least some of its activity. Addition of Benzonase to p1−381 VLPs in the presence of 0.075% SDS results in the rapid degradation of the RNA (Figure 10b). Although Benzonase will eventually digest all of the Ty-associated RNA in intact particles, it is apparent that the intact protein shell confers a substantial degree of protection against Benzonase digestion. These data are consistent with the RNA being encapsulated within a porous protein shell.

Discussion

An interesting feature of Ty-VLPs is their size variation. Most, though not all, viral capsids form structures of discrete sizes. The variation in the VLPs was most extreme for the wild-type particles, perhaps due to the presence of particles at different stages of maturation. However, it was also seen for the particles composed of the p1−381 protein alone. We do not believe that the RNA content of the particles contributes to the observed polydispersity since following complete digestion of the RNA with RNase A, the polydispersity seen by electron microscopy is retained (unpublished observations).

The polydispersity is particularly interesting given that we observed 10-fold symmetry across the size range. This suggests that polydispersity is not the result of random aggregation, but rather it is a feature of an ordered but flexible assembly process. Ten-fold symmetry is a property of icosahedral structures seen in projection along the 5-fold axis, at the resolution of the electron microscope images. However, icosahedra also show views related to the 3-fold and 2-fold axes, and we have not observed these views in Ty-VLPs. Our data are consistent with icosahedral structure for Ty-VLPs, but a three-dimensional structure analysis is needed to verify this.

The exact nature of the packing remains to be elucidated, but the combination of regularity with variation in size implies that there are local variations in subunit interactions. It has been shown that p1 is phosphorylated (Mellor *et al.*, 1985b), and it is possible that variability in post-translational modification plays a role in the variation of subunit contacts. Although the observations on the symmetry of Ty-VLPs were made using the p1−381 variant, the nature of the subunit interactions in the wild-type particles is likely to be similar. The greater polydispersity of the wild-type particles may arise not only from the presence of particles at different stages of maturation, but also from additional modes of interaction between the two protein species, p1 and p2.

Non-quasi-equivalent packing has been observed in some viruses. In the case of polyoma virus capsid, for example, both 5 and 6-fold positions are occupied by pentamers, resulting in a variety of different inter-subunit bonding geometries (Rayment *et al.*, 1982; Salunke *et al.*, 1986). This diversity is thought to be responsible for the polymorphism of polyoma viral structures seen during natural infection and *in vitro* assembly of purified components (Salunke *et al.*, 1986).

A second important feature of Ty-VLPs is their apparently open structure. We have shown using neutron scattering and the restricted access of a large nuclease (i.e. Benzonase) that the protein shell encloses the RNA, yet the RNA is accessible to the smaller nuclease, RNase A. Furthermore, similar observations of nuclease sensitivity were reported in the early

studies of reverse transcriptase reactions with detergent-treated retroviral particles (see for example Temin and Mizutani, 1970).

Nuclease sensitivity is also found in the case of cores isolated from alphaviruses (which are also enveloped viruses) such as Semliki Forest virus (Kaariainen and Soderlund, 1971; Soderlund *et al.*, 1975). Presumably, in the case of retroviruses and alphaviruses, protection of the genome in the extracellular environment is conferred by the lipid bilayer. In the case of the alphaviruses different forms of the core structure can be observed. However, these represent different stages in a highly ordered assembly process which results in monodisperse mature virions (see Fuller and Argos, 1987). This is in contrast to the situation with Ty-VLPs, at least for p1−381, where the flexibility in assembly is not part of such an assembly pathway and does not result in a homogeneous population of structures.

The formation of spherical structures which are porous, as well as polydisperse, is not without precedent and is seen, for example, in the assembly of the coated vesicle protein, clathrin. The variable size of clathrin cages is possible because of the flexible arms of the individual triskelions (Crowther and Pearse, 1981). Although we have no evidence that the assembly of Ty-VLPs occurs along similar lines, the structure of Ty-VLPs is in some respects more reminiscent of clathrin cages than of viral capsids.

The relatively unconstrained assembly of the Ty p1 protein may account for its remarkable ability to assemble even as a large fusion protein (Adams *et al.*, 1987b; Malim *et al.*, 1987). We have shown previously that we can produce hybrid Ty-VLPs from fusions at the C-terminus of p1 and that these particles are powerful antigens with implications for vaccine technology. In some cases we have added as much as 43 kDa of protein to p1 and hybrid particles have still formed efficiently.

The evolutionary divergence between Ty and retroviruses (Doolittle *et al.*, 1989) warrants caution in extrapolating the observations described here to other retroviral cores. However, the formation of some retroviral core structures, such as the cones often seen in the case of lentiviruses (see for example, Gelderblom *et al.*, 1990) cannot easily be explained in the context of quasi-equivalent packing. If variable subunit interactions are possible, the formation of conical structures is more easily envisaged.

The structural analysis of Ty-VLPs may move us closer to a more complete appreciation of their function. In considering the evidence that Ty1 VLPs (Eichinger and Boeke, 1988) and equine infectious anaemia virus (EIAV) (Roberts and Oroszlan, 1989) cores are involved in reverse transcription and integration, it is conceivable that the porous structure is essential to allow the passage of deoxynucleotide substrates into the core and to allow for a core-mediated integration event *in vivo* involving the passage of the pre-integrative DNA out of the protein shell. Such a process might substantially increase the efficiency of establishment of the provirus such that a single infecting particle leads to integration.

The symmetrical but flexible structure of Ty-VLPs combined with their porosity suggests that new rules of assembly must be devised for retrotransposon particles and perhaps for retroviral cores. Understanding these rules for this important group of genetic elements may result in a better understanding of their functional relationship with the cell.

Materials and methods

Plasmids and strains

Plasmids pMA91-10 and pMA5620 have been described previously (Dobson *et al.*, 1984; Malim *et al.*, 1987) and were used to express wild-type and p1-381 Ty-VLPs respectively (Figure 1). Both plasmids utilize phosphoglycerate kinase (PGK) promoter and termination signals and carry a *LEU 2* selectable marker gene. Yeast strain BJ2168 (a, *leu 2=*, *trp1*, *ura3-52*, *prb1-1122*, *pep4-3*, *prc1-407*) was transformed to leucine prototrophy according to the procedure of Hinnen *et al.* (1978).

Production of Ty-VLPs

Wild-type Ty1-15 and p1−381 VLPs were purified from *Saccharomyces cerevisiae*, strain BJ2168, transformed with plasmids pMA91-10 and pMA5620 respectively. The method for the purification of the particles has been described in detail elsewhere (Burns *et al.*, 1991). Briefly, 16 l of culture were harvested and the cells broken by agitation with glass beads. The particles were purified from a clarified lysate by a combination of differential centrifugation, rate zonal centrifugation and size exclusion chromatography.

Electron microscopy

Ty-VLPs on thin carbon support films were negatively stained with 2% uranyl acetate. Micrographs were taken with low electron dose, with no irradiation of the specimen area before the photographic exposure, on a Philips 400T or a JEOL 1200EX electron microscope. Specimens negatively stained on holey carbon films (Toyoshima, 1989) were photographed under conventional dose conditions. For cryo EM, a thin film of the VLP suspension was vitrified by plunging into ethane slush (Dubochet *et al.*, 1988) and photographed on a Philips 420T microscope using a Gatan cryotransfer holder. The electron dose was ~1000 e/nm^2 and the underfocus 1−2 μm. In all cases the operating voltage was 120 kV, and the micrographs were recorded on Agfa 23D56 film at a magnification of 36 000 or 40 000 ×.

Image processing

We are currently developing a novel laser digitizer based on a Bio-Rad MRC500 scanning system. This instrument was used to scan interactively the low dose electron microscopy films of VLPs and digitize particles in 11 μm steps over a field of 2.75 mm^2, giving a 256 × 256 pixel particle image. Sixteen to thirty two 1 s scans were accumulated into an average scanned image. Satisfactory geometric linearity and field evenness were ensured by using a scanned microscope graticule for digital correction. Digitized images were processed using the Semper 6 Plus image processing system (Synoptics Ltd, Cambridge, UK) on an 80386 microcomputer. Films recorded at normal dose, of particles negatively stained on holey grids, were digitized on a drum scanner (Optronics or Scandig) with 25 μm pixel size. Particle radii and centres were estimated by choosing three points on the outer edge of the particle (position of maximum stain density, or of maximum contrast between protein and ice density, including visible projections) and fitting a circle through the three points, which was acceptable if it symmetrically enclosed the particle. Repeating this procedure for circularly symmetric particles gave radii which were reproducible within ±5%, and centre positions which did not vary by more than two pixels. Most of the large wild-type particles were distorted into elliptical shapes. In these cases, radii were estimated more roughly by averaging maximum and minimum values for a particle. The accuracy of the radius histograms was checked by comparing independent measurements on the same set of particles. Details of the distribution varied slightly, but the means and ranges of the distributions agreed within 5%.

Low dose images of p1−381 particles negatively stained on carbon films were assessed for rotational symmetry by calculating the radially weighted rotational auto-correlation (Saxton, 1978). This function ranges from −1 to 1 but does not necessarily oscillate about a mean value of zero. A correlation coefficient of 1 indicates perfect correlation, zero indicates no correlation and −1 indicates exact anti-correlation (i.e. reversed contrast). The annulus containing the part of the structure used in the rotational analysis is shown in Figure 11.

Hydrodynamic methods

Analytical ultracentrifugation was performed using a Beckman Model E centrifuge, at a speed of 7928 r.p.m. The p1−381 VLPs were in 140 mM NaCl, 1 mM EDTA, 10 mM Tris−HCl, pH 7.6 (TEN) at concentrations between 0.31 and 0.94 mg/ml at 16°C.

Photon correlation spectroscopy was performed using a Coulter electronics Model N4 sub-micron particle size analyser. VLPs were at a concentration of 250 μg/ml in TEN.

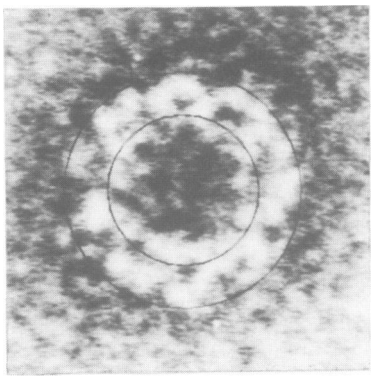

Fig. 11. Region used to calculate rotational correlations. The negatively stained Ty-VLP from Figure 5d is shown with rings of radius 10.5 and 16.5 nm superimposed, to show the annular region used in calculating the rotational correlation.

Nuclease digestions

All measurements were made using a Perkin-Elmer Lambda 2 spectrophotometer. The nucleases used were DNase 1 (FPLC pure, Pharmacia, Sweden), pancreatic RNase A (Pharmacia, Sweden) and Benzonase (ultra-pure grade, Benzon Pharma, Denmark). Reactions were performed at room temperature in TEN containing 3 mM $MgCl_2$. Nucleic acid degradation was observed by measuring the increase in absorbance at 260 nm. Sedimentation of VLPs was achieved by centrifugation at 540 000 *g* for 30 min using a TLA-100.3 rotor (Beckman).

Neutron scattering

Measurements were made at the small angle diffractometer D11 at the Institut Laue-Langevin, Grenoble (Ibel, 1976). pl−381 VLPs were observed at concentrations between 0.6 and 7 mg/ml, as determined by quantitative amino acid analysis, in 140 mM NaCl, 1 mM EDTA and 10 mM Tris−HCl/DCl pH/pD 7.4, at 10°C. Scattering intensities were recorded at sample-to-detector lengths of 2.25−20 m. Solvent and detector backgrounds were subtracted prior to radial averaging of the data. Calculated scattering profiles were generated from spherical shell models by the program SSQFUN using the experimentally determined maximum dimension and radius of gyration to constrain outer particle dimension and total scattering mass respectively. Although a theoretical analysis of the effect of polydispersity on neutron scattering profiles has been performed, its rigorous application requires a quantitative description of the polydispersity (Glatter, 1980; Cusack *et al.*, 1983). Alternatively, a less rigorous, but simpler, approximation can be made by increasing the apparent wavelength spread of the incident beam. Given the available data, we consider the latter approach is more realistic. Therefore, the wavelength spread ($\Delta\lambda/\lambda$) used in these calculations was 0.2 rather than the actual value of 0.08, and only simple, low resolution models were considered. The same instrumental smearing parameters were used for each fit although these are not rigorously equivalent to the physical parameters of the instrument. For the beam divergence a compromise value was used to account for the fact that the curves are composites from the different collimation conditions.

Acknowledgements

We thank Dr David Stuart, Dr Laurence Pearl and Dr Walter Gratzer for helpful discussions. We thank the Institut Laue-Langevin for provision of neutron scattering facilities and in particular Dr R.E.Ghosh for making available the SSQFUN program. We are very grateful to Dr David Stokes for help with all aspects of cryo-electron microscopy at Cambridge MRC Laboratory of Molecular Biology, and to Dr Richard Henderson and Dr Nigel Unwin for making the equipment available. We also thank Dr Ed Morris and Dr David Stuart for use of drum scanners at Imperial College and Oxford University and help with data transfer programs. We thank Troels Sorensen and David Botchinsky for help with particle measurements. We thank Bio-Rad Microscience Ltd for providing equipment and technical advice, the SERC for support to N.S.W. and the MRC for support to H.R.S.

References

Adams,S.E., Mellor,J., Gull,K., Sim,R.B., Tuite,M.F., Kingsman,S.M. and Kingsman,A.J. (1987a) *Cell*, **49**, 111−119.
Adams,S.E., Dawson,K.M., Gull,K., Kingsman,S.M. and Kingsman,A.J. (1987b) *Nature*, **329**, 68−70.
Boeke,J.D., Garfinkel,D.J., Styles,C.A. and Fink,G.R. (1985) *Cell*, **40**, 491−500.
Bowerman,B., Brown,P.O., Bishop,J.M. and Varmus,H.E. (1989) *Genes. Dev.*, **3**, 469−478.
Burns,N.R., Gilmour,J.E.M., Kingsman,S.M., Kingsman,A.J. and Adams,S.E. (1991) *Methods Mol. Biol.*, **8**, 277−285.
Bushman,F.D., Fugiwara,T. and Craigie,R. (1990) *Science*, **249**, 1555−1558.
Craigie,R., Fugiwara,T. and Bushman,F. (1990) *Cell*, **62**, 829−837.
Crowther,R.A. and Pearse,B.M.F. (1981) *J. Cell Biol.*, **91**, 790−797.
Cusack,S., Oostergetel,G.T., Krijgsman,P.C.J. and Mellema,J.E. (1983) *J. Mol. Biol.*, **171**, 139−155.
Dobson,M.J., Mellor,J., Fulton,A.M., Roberts,N.A., Bowen,B.A., Kingsman,S.M. and Kingsman,A.J. (1984) *EMBO J.*, **3**, 1115−1119.
Doolittle,R.F., Feng,D.F., Johnson,M.S. and McClure,M.A. (1989) *Q. Rev. Biol.*, **64**, 1−30.
Dubochet,J., Adrian,M., Chang,J.J., Homo,J.C., Lepault,J., McDowall,A. and Shultz,P. (1988) *Q. Rev. Biophys.*, **21**, 129−228.
Eichinger,D.J. and Boeke,J.D. (1988) *Cell*, **54**, 955−966.
Fuller,S.D. and Argos,P. (1987) *EMBO J.*, **6**, 1099−1105.
Gelderblom,H.R., Marx,P.A., Vzel,M., Gheysen,D., Munn,R.J., Joy,K.I. and Pauli,G. (1990) In *Retroviral Proteases: Maturation and Morphogenesis*. Macmillan, London, pp. 159−180.
Glatter,O. (1980) *J. Appl. Crystallogr.*, **13**, 1−11.
Glatter,O. (1982) In Glatter,O. and Kratky,O. (eds), *Small Angle X-ray Scattering*. Academic Press, London, p. 181.
Guinier,A. and Fournet,G. (1955) *Small Angle Scattering of X-rays*. Wiley, New York.
Hinnen,A., Hicks,J.B. and Fink,J.R. (1978) *Proc. Natl Acad. Sci. USA*, **75**, 1929−1933.
Ibel,K. (1976) *J. Appl. Crystallogr.*, **9**, 630−643.
Jacrot,B. and Zaccai,G. (1981) *Biopolymers*, **20**, 2413−2426.
Katz,R.A., Merkel,G., Kulkosky,J., Leis,J. and Skalka,A.M. (1990) *Cell*, **63**, 87−95.
Kaarrianen,L. and Soderlund,H. (1971) *Virology*, **43**, 291−299.
Kingsman,A.J. and Kingsman,S.M. (1988) *Cell*, **53**, 333−335.
Malim,M.H., Adams,S.E., Gull,K., Kingsman,S.M. and Kingsman,A.J. (1987) *Nucleic Acids Res.*, **15**, 7571−7580.
Mellor,J., Malim,M.H., Gull,K., Tuite,M.F., McCready,S. Dibbayawan,T., Kingsman,S.M. and Kingsman,A.J. (1985a) *Nature*, **318**, 583−586.
Mellor,J., Fulton,A.M., Dobson,M.J., Roberts,N.A., Wilson,W., Kingsman,A.J. and Kingsman,S.M. (1985b) *Nucleic Acids Res.*, **13**, 6249−6363.
Rayment,I., Baker,T.S., Caspar,D.L.D. and Murakami,W.T. (1982) *Nature*, **295**, 110−115.
Roberts,M.M. and Oroszlan,S. (1989) *Biochem. Biophys. Res. Commun.*, **160**, 486−494.
Salunke,D.M., Caspar,D.L.D. and Garcea,R.L. (1986) *Cell*, **46**, 895−904.
Saxton,W.O. (1978) *Computer Techniques for Image Processing in Electron Microscopy*. Academic Press, pp. 201−203 and 218−219.
Soderlund,H., Kaarrianen,L. and von Bondsdorff,C.-H. (1975) *Med. Biol.*, **53**, 412−417.
Svedberg,T. and Pederson,K.O. (1940) *The Ultracentrifuge*. Oxford University Press, London.
Temin,H.M. and Mizutani,S. (1970) *Nature*, **226**, 1211−1213.
Timmins,P.A. and Zaccai,G. (1988) *Eur. Biophys. J.*, **15**, 257−269.
Toyoshima,C. (1989) *Ultramicroscopy*, **30**, 439−444.

Received on August 28, 1991; revised on November 18, 1991